ELSEVIER

International Journal of Mass Spectrometry 226 (2003) 211–222

International Journal of Mass Spectrometry

www.elsevier.com/locate/ijms

Thermodynamic control of final ion distributions in MALDI: in-plume proton transfer reactions

K. Breuker[1], R. Knochenmuss[2], J. Zhang, A. Stortelder[3], R. Zenobi*

Department of Chemistry, Swiss Federal Institute of Technology (ETH), Hönggerberg HCI, CH-8093 Zürich, Switzerland

Received 26 July 2001; accepted 12 August 2002

Dedicated to Prof. Franz Hillenkamp on the occasion of his 65th birthday.

Abstract

Gas-phase thermochemical data on matrix-assisted laser desorption/ionization (MALDI) matrix species were used to calculate the energetics of possible proton transfer reactions. These were investigated for the MALDI matrices 2,4,6-trihydroxyacetophenone and sinapic acid, with the tripeptide glycyl–glycyl–histidine as analyte. MALDI proton transfer product ion distributions were found to be predicted by the energetics of possible secondary ion–molecule reactions, at all laser fluences sufficient to generate a dense plume. Near the ion generation fluence threshold, the mass spectra deviate from the thermodynamic predictions. This shows that the MALDI plume exhibits both thermodynamically and kinetically controlled regimes, depending on desorption conditions. Possible thermal ground state proton transfer primary ionization pathways were also considered, and found to be inconsistent with the data.

Keywords: MALDI; Ionization; Gas-phase basicity; Proton transfer reactions; Thermochemistry

1. Introduction

Matrix-assisted laser desorption/ionization (MALDI) [1–3] has become an indispensable tool for biomolecular analysis, and the mechanisms by which both the primary and the final, observed ions form are currently of much interest [4–9]. The hope is that, with deeper understanding, MALDI can be rationally and systematically developed, and that the outcome of MALDI experiments can be predicted and planned. Practical consequences could be greater sensitivity, wider applicability, better reproducibility, and possibly quantitative measurements.

As recently described [10], MALDI ionization mechanisms can be divided into primary and secondary ionization steps. By primary steps we mean those processes converting neutral reactants into charged products by action of the laser pulse on the sample. These include multi-photon ionization, energy pooling mechanisms, disproportionation reactions, excited-state proton transfer, thermal ionization, desorption of preformed ions, and break-up of the sample into charged chunks and clusters [10]; these

* Corresponding author.
E-mail address: zenobi@org.chem.ethz.ch (R. Zenobi).
[1] Present address: Department of Chemistry, University of Innsbruck, Innsbruck, Austria.
[2] Co-corresponding author. Present address: Novartis Pharma AG, WSJ-503.1104, CH-4002 Basel, Switzerland.
E-mail address: rknochenmuss@gmx.net
[3] Present address: Department of Analytical Chemistry and Applied Spectroscopy (ACAS), Faculty of Sciences, Vrije Universiteit Amsterdam, de Boelelaan 1083, 1081 HV Amsterdam, The Netherlands.

1387-3806/02/$ – see front matter
PII S1387-3806(02)00965-X

are not the subject of the present study. The primary steps may differ significantly for infrared and ultraviolet desorption/ionization.

Secondary steps are any subsequent ion–molecule reactions that convert the initial charged species to the ions that are observed at the detector. These may involve proton transfer, electron transfer, and cation attachment or transfer. As proposed in [7], primary ionization may be partially or completely masked by such secondary reactions. While this complicates elucidation of the primary ionization steps, it explains the similarity of MALDI spectra recorded under different conditions, and provides a framework for predicting MALDI mass spectra. Because thermochemical data for matrix and analytes are becoming more available [7,11–25] these hypotheses are increasingly subject to experimental test.

A more comprehensive discussion of secondary ion–molecule reactions in MALDI can be found in a recent article [7]; here we present a case study supporting the concepts presented therein, for systems in which proton transfer reactions are dominant. The present study is concerned *only* with proton transfer reactions. Other ions are often observed in MALDI, particularly metal adduct ions and matrix radical species. The minor quantities of such ions which can be found in the systems studied here are not treated in detail because not enough thermodynamic information is known, and because they are clearly far less important than the protonated or deprotonated species.

Systems were chosen for this study in which Gibbs free energies of matrix–matrix and matrix–analyte proton transfer reactions are known or were determined experimentally. This allows us to test the hypothesis that thermochemistry determines the final ion distributions as a result of efficient secondary reactions in the plume. Experimental conditions were also chosen so as to most clearly test the hypothesis. For investigating matrix–analyte reactions, samples were prepared by mixing matrix and analyte in molar ratios of as high as 1:1. Such high analyte concentrations are not typically used in MALDI experiments, but were chosen here to ensure that reactions are not limited by quantities of reactants. Under these conditions, complete suppression of all matrix ions in the mass spectrum can be observed. This “matrix suppression effect,” has been studied in some detail [7,26–28]. Because MALDI plume density and therefore the number of collisions can be expected to increase with increasing laser fluence, the effect of fluence on relative ion yields was also investigated.

2. Experimental

Experiments were performed on a Fourier transform ion cyclotron resonance (FT-ICR) mass spectrometer with a 4.69 T superconducting magnet (Bruker, Fällanden, Switzerland). The rf electronics and Odyssey data acquisition system were from Finnigan (Finnigan FT–MS, Madison, WI, USA). The laboratory-built vacuum system was comprised of a closed cylindrical ion cell of unit aspect ratio and a sample transfer device for insertion of solid material. The instrument operating pressure was below 10^{-8} mbar. The metal target supporting the solid MALDI samples was positioned approximately 15 mm from the cell. A Nd:YAG laser (Continuum, Minilite ML-10, Santa Clara, CA, USA) operated at 355 nm was used for laser desorption/ionization.

Upon laser desorption/ionization, ions were ejected from the solid samples and drifted into the cell volume. The electric potential on the trapping plates was then raised to $+4$ or -4 V, depending on the ion polarity to be trapped. The drift time of the ions was chosen to maximize the number of trapped ions, which was 50 ms for 2,4,6-trihydroxyacetophenone and 100 ms for sinapic acid. After a 1 ms cooling delay during which the ions were allowed to axialize, the trapping potential was lowered to $+2$ or -2 V. The ions were then excited to larger cyclotron radii by employing a chirp waveform and detected. Spectra from single laser shots were collected at each fluence.

The laser pulse energy on the sample was controlled by varying the time delay between the flashlamp and the Q-switch triggers. This delay was calibrated against the laser energy using a pyroelectric detector inserted into the beam. The laser spot size on the target

was estimated from sample ablation profiles to be about 2×10^{-6} m^2, from which laser fluences were calculated. In the experiments reported in this study, these ranged from 200 to 600 J/m^2. Typical fluences in ultraviolet MALDI are somewhat lower, between 50 and 300 J/m^2 [29]. However, the higher fluences were only needed in the experiments with a matrix–analyte concentration of 1:1, but not when pure matrix or lower analyte concentrations were used.

The tripeptide glycyl–glycyl–histidine (abbreviated GGH; from Aldrich, Buchs, Switzerland) was used as a model analyte together with the MALDI matrices 2,4,6-trihydroxyacetophenone (THAP; from Aldrich, Buchs, Switzerland) and sinapic acid (SA; from Fluka, Buchs, Switzerland). Matrix–analyte solutions were prepared by mixing matrix and analyte solutions (0.05 M each, in acetonitrile/water mixture 1:2 by volume) in a glass vial. The solid samples were prepared by successively placing 5 μL drops on the target (about 50 μL total) and drying until a relatively thick layer of matrix or matrix–analyte crystals completely covered the metal surface. Co-crystallization was somewhat critical for the SA/GGH sample, and a glass slide was used to crush and grind the wet crystals before the last drop deposited had dried, to obtain a good mixing of matrix and analyte.

Several factors motivated the choice of the analyte glycyl–glycyl–histidine. First, its gas-phase basicity is known and lies above those of the matrices used [10,30,31], making proton transfer from protonated matrix to neutral GGH an exoergic reaction. Second, this tripeptide does not exhibit a significant absorption at the wavelengths used, and the laser energy is primarily absorbed by the matrix molecules. Third, its mass (269 Da) is comparable to those of the matrix species, minimizing possible mass discrimination effects in FT-ICR trapping efficiency.

The GB of $[GGH - H]^-$ has not been precisely determined, but the exact value is less important here than its GB relative to those of deprotonated THAP and SA. Proton competition experiments were performed to bracket the GB of deprotonated GGH, and show that it lies between deprotonated THAP and SA. First, $[GGH - H]^-$ was isolated and collisionally cooled (300 K) with nitrogen gas in the FT-ICR cell prior to reaction with neutral THAP evaporated from a solid sample. Using the exoergic (DG = −105 kJ/mol) reference reaction between acetate (GB = 1429 kJ/mol) [32] and THAP as described previously [11], it was verified that the GB of deprotonated GGH lies significantly above that of deprotonated THAP (1324 kJ/mol) [12]. In a similar experiment with another reference base, 2-amino-5-nitropyridine (ANP), it was found that the GB of deprotonated GGH lies below that of deprotonated ANP, or 1399 kJ/mol [12]. The GB of deprotonated GGH was therefore experimentally bracketed between that of $[THAP - H]^-$ and $[SA - H]^-$ (GB = 1400 kJ/mol [11], very close to that of ANP).

3. Results and discussion

3.1. Matrix suppression effect with THAP matrix and GGH analyte

Fig. 1 shows the mass spectra of THAP alone and with GGH analyte, in both positive and negative modes. A matrix suppression effect [7,26–28] is observed in positive mode, analogous to that found for numerous other matrix–analyte pairs [27,28]. As is often the case with the matrix suppression effect, the matrix–analyte ion intensity ratio shows a step-like approach to suppression at high analyte concentration. GGH being a relatively low molecular weight analyte, the suppression concentration ratio is less than 10, consistent with other small analytes [28]. As proposed in [7,27,28], it should be possible to understand this effect in terms of primary ion generation processes and/or secondary ion–molecule reactions in the plume. We next consider the latter in detail, and find that they are sufficient to describe the observed effects.

3.2. THAP/GGH secondary proton transfer reactions

Fig. 1(a) shows the mass spectra of THAP obtained with 355 nm irradiation. The most abundant ions are

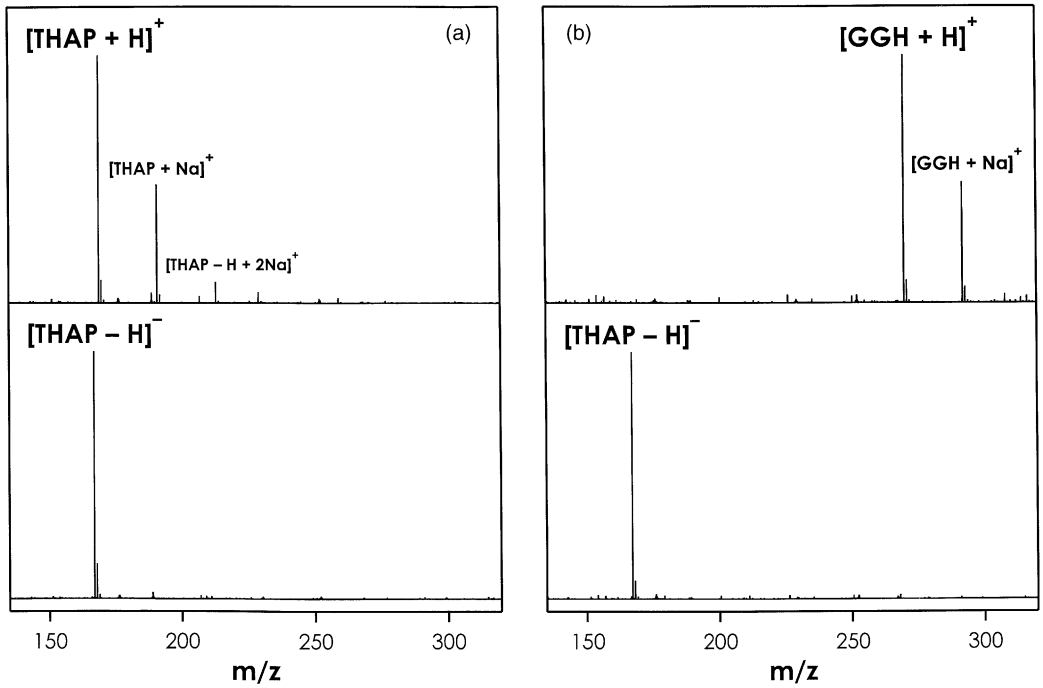

Fig. 1. Laser desorption/ionization FT-ICR mass spectra obtained from 2,4,6-trihydroxyacetophenone (a), and a mixture of 2,4,6-trihydroxyacetophenone and glycyl–glycyl–histidine (1:1 molar ratio) (b), in positive (upper traces) and negative (lower traces) polarity. The laser fluence was 300 J/m^2 in (a) and 360 J/m^2 in (b).

protonated and deprotonated THAP in positive and negative polarity, respectively. These can further react in secondary proton transfer reactions with analyte, if present.

The proton affinity of the THAP matrix has been determined to be 882 kJ/mol [33]. Because typical entropy contributions at 300 K are ~30 kJ/mol [30], GB(THAP) should be close to 850 kJ/mol. The GB of the neutral tripeptide GGH is much higher, 980 kJ/mol [30], so that reaction (1.1) of Table 1 is exoergic by 130 kJ/mol. The gas-phase basicity of deprotonated THAP, GB([THAP − H]$^-$), was determined to be 1324 kJ/mol [12]. The GB of [GGH − H]$^-$ was shown to be higher, as noted above. Thus, reaction (1.2) (which could not be probed directly due to the negligible vapor pressure of GGH) must be endoergic.

The matrix suppression effect of Fig. 1(b) is consistent with the thermodynamics of these reactions: protonated THAP can react with neutral GGH to form [GGH + H]$^+$, but [THAP − H]$^-$ will not be able to deprotonate GGH. Using a matrix–analyte ratio of 1:1, protonated GGH and deprotonated THAP are the main ions detected in positive and negative mode, respectively. The high analyte concentration and the favorable thermodynamics give rise to complete suppression of matrix signals in the positive ion spectrum, accompanied by a strong matrix signal in the negative polarity.

Table 1
Possible secondary ion formation proton transfer reactions for GGH as analyte and THAP as matrix

Secondary ion formation PT reaction	ΔG (kJ/mol)
(1.1) GGH + [THAP + H]$^+$ $\overset{\Delta G}{\rightarrow}$ [GGH + H]$^+$ + THAP	−130
(1.2) [THAP − H]$^-$ + GGH $\overset{\Delta G}{\rightarrow}$ THAP + [GGH − H]$^-$	Endoergic <+75

ΔG denotes the corresponding free energy changes at 300 K.

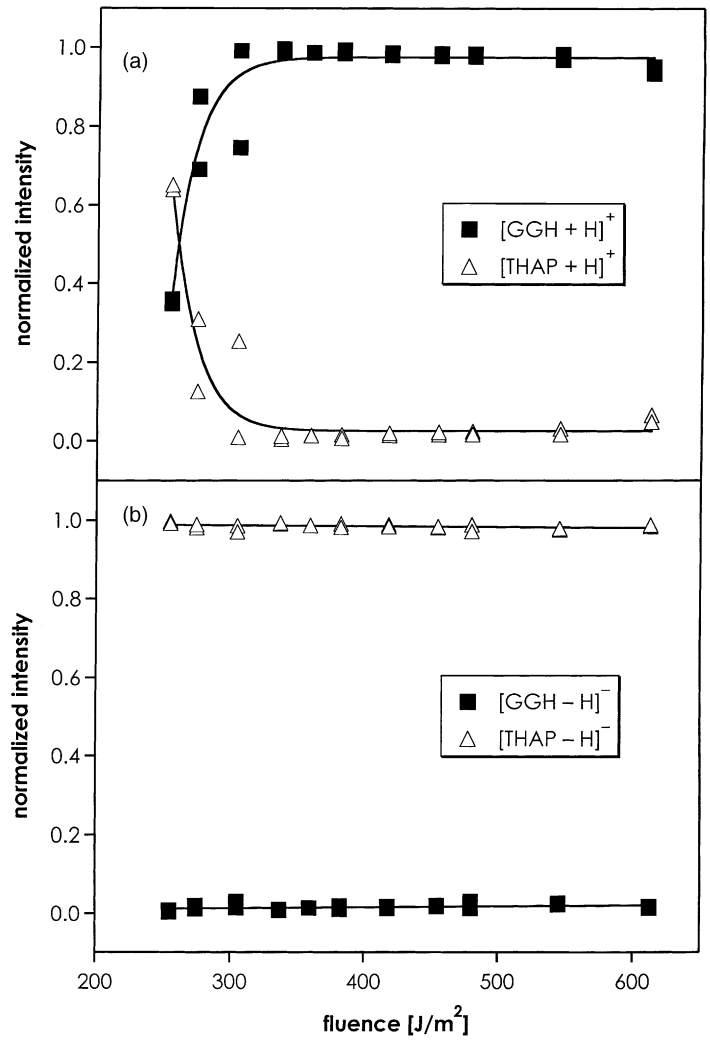

Fig. 2. Normalized intensities of MALDI ion species obtained from a 2,4,6-trihydroxyacetophenone/glycyl–glycyl–histidine sample (1:1 molar ratio); (a) positive ions, (b) negative ions, as a function of laser fluence. Solid lines are to guide the eye.

The spectra in Fig. 1(b) were obtained using a laser fluence of 360 J/m^2. When using lower laser fluences, the relative matrix ion abundances were higher and up to 65%, as shown in Fig. 2. With increasing fluence, the matrix signals disappeared and protonated analyte became the only product in positive polarity, consistent with the thermochemistry of reaction (1.1). Only matrix ions were detected in the negative polarity, independent of the fluence applied. This is also consistent with thermochemistry (reaction (1.2)).

These data indicate that with increasing laser fluence and plume density, an increasing number of collisions between protonated matrix and neutral analyte allow for secondary proton transfer via reaction (1.1), and ion–molecule equilibrium is established. At lower fluences there is incomplete reaction, and matrix precursor ions are more numerous. We interpret this as a transition from a kinetically limited regime (at low plume density) to thermodynamic equilibrium (at high plume density).

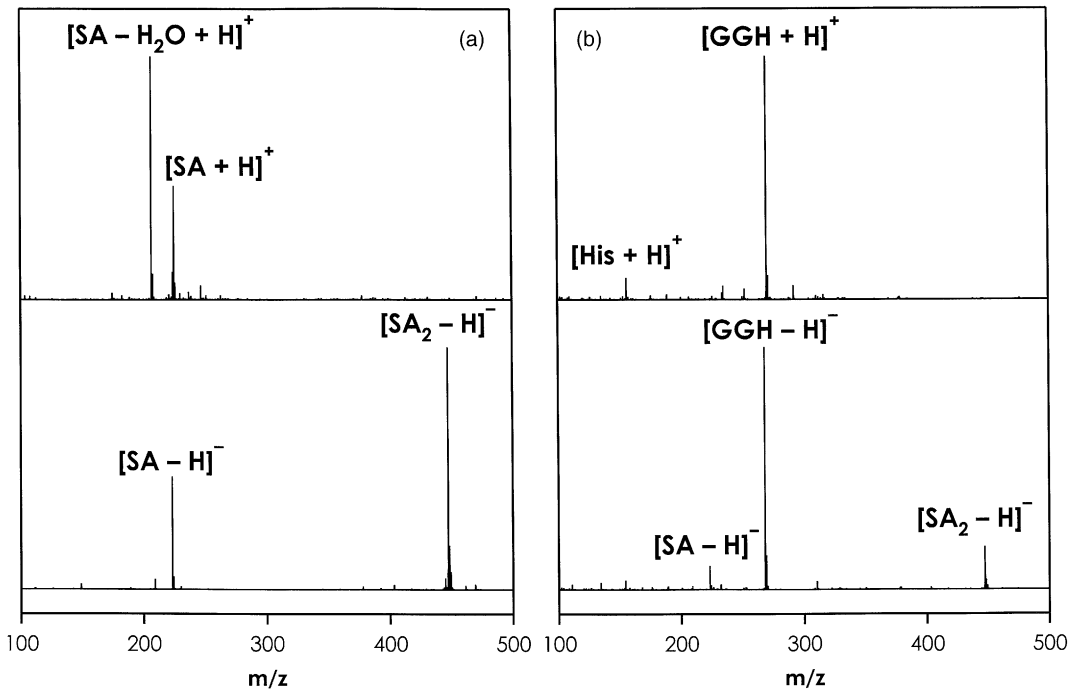

Fig. 3. Laser desorption/ionization FT-ICR mass spectra obtained from sinapic acid (a), and a mixture of sinapic acid and glycyl–glycyl–histidine (1:1 molar ratio) (b), in positive (upper traces) and negative (lower traces) polarity. The laser fluence was 300 J/m^2 in (a) and 380 J/m^2 in (b).

3.3. SA/GGH secondary proton transfer reactions

A system characterized by a more complex thermochemistry is glycyl–glycyl–histidine together with the MALDI matrix SA. This is largely because there are more ions derived from the matrix than is the case for THAP, as shown in Fig. 3(a).

Besides protonated matrix, a protonated fragment ion due to loss of H_2O is typically observed in positive polarity. In negative polarity, deprotonated monomeric and dimeric matrix, $[SA-H]^-$ and $[SA_2-H]^-$, are the most prominent ions. The corresponding gas-phase basicities were determined to be GB(SA) = 861 kJ/mol [15], GB[SA − H_2O] = 901 kJ/mol [15], GB([SA − H]$^-$) = 1400 kJ/mol [11], and GB([SA_2 − H]$^-$) = 1285 kJ/mol [11]. Because more types of matrix ions are observed with SA than with THAP, the number of possible matrix–matrix and matrix–analyte reactions is also larger, as shown in Table 2.

Table 2
Possible secondary ion formation proton transfer reactions for GGH as analyte and SA as matrix

Secondary ion formation PT reaction	ΔG (kJ/mol)
(2.1) $[SA+H]^+ + F \overset{\Delta G}{\rightarrow} SA + [F+H]^+$	−40
(2.2) $[SA-H]^- + SA_2 \overset{\Delta G}{\rightarrow} SA + [SA_2-H]^-$	−115
(2.3) $GGH + [SA+H]^+ \overset{\Delta G}{\rightarrow} [GGH+H]^+ + SA$	−120
(2.4) $GGH + [F+H]^+ \overset{\Delta G}{\rightarrow} [GGH+H]^+ + F$	−80
(2.5) $[SA_2-H]^- + GGH \overset{\Delta G}{\rightarrow} SA_2 + [GGH-H]^-$	Endoergic <+115
(2.6) $[SA-H]^- + GGH \overset{\Delta G}{\rightarrow} SA + [GGH-H]^-$	Exoergic >−75

F is a matrix fragment resulting from loss of H_2O. ΔG denotes the corresponding free energy changes at 300 K.

Again, the exact energetics of the reactions involving $[GGH - H]^-$ are not known, although the relative GBs are known. $[SA_2 - H]^-$ is an even weaker base than $[THAP - H]^-$, so reaction (2.5) must be endoergic. Also $[GGH - H]^-$ is less basic than $[ANP - H]^-$ (GB = 1399 kJ/mol) so reaction (2.6) with $[SA - H]^-$ (GB = 1400 kJ/mol) is exoergic.

The secondary matrix–matrix reactions (2.1) and (2.2) are both exoergic. For a pure SA sample, thermochemistry then predicts $[F + H]^+$ ($F = SA - H_2O$) and $[SA_2 - H]^-$ to be the most intense signals, in agreement with the data shown in Fig. 3(a). Analyte protonation can proceed via reactions (2.3) and (2.4), and deprotonation via reaction (2.6). Given that sufficient collisions occur, protonated GGH should be the major product in positive polarity, and deprotonated GGH should be formed via reaction (2.6). This agrees well will the spectra shown in Fig. 3(b), but as already observed with the THAP/GGH system, this is true only for laser fluences somewhat above threshold. At lower fluences, in the kinetically limited regime, mainly matrix ions were detected with the SA/GGH system, as illustrated in Fig. 4.

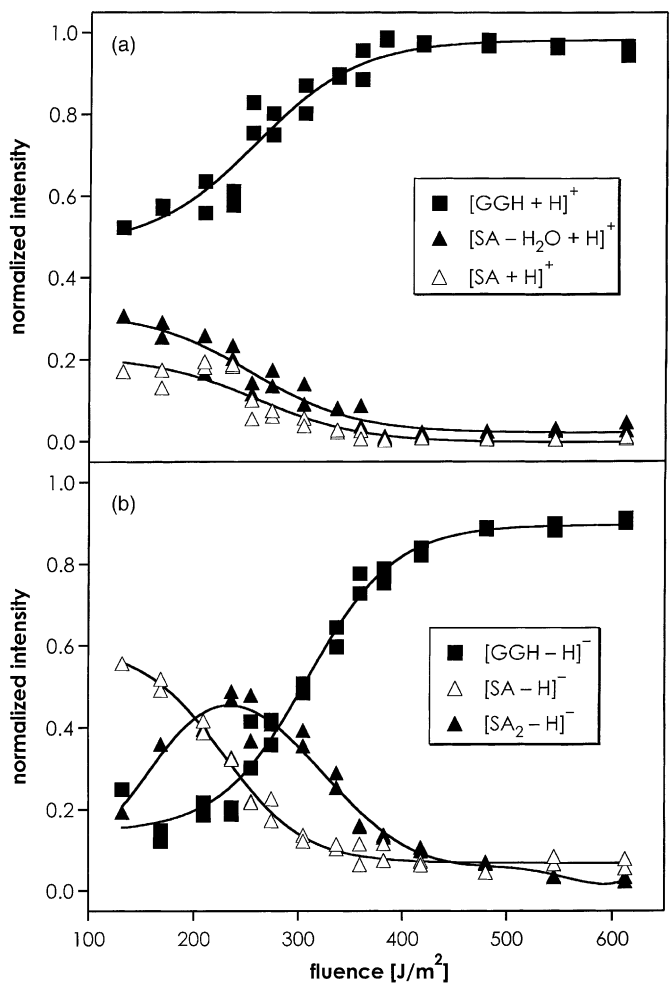

Fig. 4. Normalized intensities of MALDI ion species obtained from a sinapic acid/glycyl–glycyl–histidine sample (1:1 molar ratio), (a) positive ions, (b) negative ions, as a function of laser fluence. Solid lines are to guide the eye.

The dependence of relative intensities on fluence is more complex here than for the THAP/GGH system, but can be explained using similar thermodynamic arguments. At fluences below 200 J/m^2, mainly monomeric matrix species are observed. With increasing fluence, secondary reactions between protonated matrix and neutral analyte become frequent (reactions (2.3) and (2.4)), and matrix suppression starts to occur in positive polarity. In negative polarity, $[SA - H]^-$ reacts with neutral SA dimers to form $[SA_2 - H]^-$ via reaction (2.2), indicating that ion–molecule equilibrium conditions are approached.

Nevertheless, the relative $[SA_2 - H]^-$ intensity reaches only a local maximum at about 250 J/m^2. Collision-induced dissociation (CID) experiments revealed that the $[SA_2 - H]^-$ ion formed upon laser desorption/ionization is a non-covalently bound complex of SA and $[SA-H]^-$, with a dissociation onset at about 1.3 eV. Energetic ion/neutral collisions in the MALDI plume are sufficient to dissociate this complex. At fluences not too close to threshold, plume densities and collision rates are high enough to largely dissociate $[SA_2 - H]^-$. The product ions are $[SA - H]^-$, which in turn exoergically react with neutral tripeptide to form $[GGH - H]^-$. Whereas the $[SA_2 - H]^-$ ion with a basicity of 1285 kJ/mol will not be able to abstract a proton from the tripeptide GGH (reaction (2.5)), the GB of $[SA - H]^-$ is 1400 kJ/mol and sufficiently high to promote tripeptide deprotonation (reaction (2.6)). In other words, dissociation of $[SA_2 - H]^-$ provides reactants for the secondary reaction (2.6), and the unusual phenomenon of simultaneous positive and negative matrix suppression is observed at fluences above 400 J/m^2.

Proton transfer from SA_2 to $[GGH - H]^-$, the reverse of reaction (2.5), is energetically favorable, but cannot proceed at fluences above 250 J/m^2 because neutral matrix dimers will undergo the fate of their ionic counterparts and be dissociated by energetic collisions. In contrast, in the kinetically controlled regime below 250 J/m^2, reaction (2.6) does not proceed to completion due to insufficient collisions.

3.4. Primary ionization mechanisms: ground-state proton disproportionation and matrix suppression

The MALDI mass spectra shown here are predicted by the thermodynamics of the relevant secondary proton transfer reactions. However, ion distributions and matrix suppression could arise from thermodynamically controlled primary ionization processes as well [27]. If primary ionization directly leads to the energetically most favorable gas-phase ions, then no secondary matrix–analyte ion–molecule reactions are necessary (or favorable). The fluence dependencies shown in Figs. 2 and 4 strongly suggest that the primary ions are not those finally observed in these systems (if enough collisions occur). However, the question remains—to what extent can primary mechanisms contribute to the observed spectra?

Possible primary ionization proton disproportionation reactions and the corresponding free energies are summarized in Table 3 for the THAP/GGH and the SA/GGH systems. Matrix–matrix reactions are endoergic by only 385 kJ/mol (reaction (3.6)) to 540 kJ/mol (reaction (3.3)). Matrix–analyte reactions can be even less costly; proton transfer from neutral dimeric SA to neutral GGH requires only 305 kJ/mol (reaction (3.8)). This should be compared to typical

Table 3
Possible primary ion formation proton transfer reactions for GGH as analyte and THAP and SA as matrix

Primary ion formation PT reactions	ΔG (kJ/mol)
(3.1) $THAP + THAP \xrightarrow{\Delta G} [THAP + H]^+ + [THAP - H]^-$	470
(3.2) $GGH + THAP \xrightarrow{\Delta G} [GGH + H]^+ + [THAP - H]^-$	345
(3.3) $SA + SA \xrightarrow{\Delta G} [SA + H]^+ + [SA - H]^-$	540
(3.4) $F + SA \xrightarrow{\Delta G} [F + H]^+ + [SA - H]^-$	500
(3.5) $SA + SA_2 \xrightarrow{\Delta G} [SA + H]^+ + [SA_2 - H]^-$	425
(3.6) $F + SA_2 \xrightarrow{\Delta G} [F + H]^+ + [SA_2 - H]^-$	385
(3.7) $GGH + SA \xrightarrow{\Delta G} [GGH + H]^+ + [SA - H]^-$	420
(3.8) $GGH + SA_2 \xrightarrow{\Delta G} [GGH + H]^+ + [SA_2 - H]^-$	305

F is a matrix fragment resulting from loss of H_2O. ΔG denotes the corresponding free energy changes at 300 K.

ionization potentials of matrix molecules in the range of 750–800 kJ/mol [10,34,35].

Reaction (3.2) is substantially less endoergic than (3.1), which predicts matrix suppression in positive mode, as observed. However, it also predicts that matrix suppression should appear at all fluences for this sample, if it occurs via a primary ionization mechanism. From Fig. 2 we see that this is clearly not the case. At low fluence, the mass spectra are much more consistent with reaction (3.1), in spite of its greater endoergicity.

For SA matrix, reaction (3.8) is the least costly, and consistent with the middle fluence range of Fig. 4. (The higher fluence range appears to be dominated by CID of the SA dimer, and is not relevant here.) Again, however, this pattern should continue at low fluence if primary mechanisms are the determining factor. Instead, the low fluence ions are more consistent with reaction (3.7).

From these considerations, it seems likely that secondary mechanisms are indeed largely responsible for the final ions observed in these experiments. The role of ground state primary ionization proton disproportionation pathways like reactions (3.1) through (3.8) is very limited due to their purely thermal nature. They are endoergic by >300 kJ/mol, and temperatures much higher than room temperature would be needed to promote them. For a system at thermal equilibrium, Fig. 5 shows the calculated fraction of molecules with thermal energies higher than a threshold reaction endoergicity, E_0, as a function of temperature (Eq. (1)). In other words, the maximum fraction of molecules that could react on to ions at a given temperature can be calculated using Eq. (1):

$$\frac{N(E > E_0)}{N_{\text{total}}} = \frac{\int_{E_0}^{\infty} \exp(-E/kT)\,\mathrm{d}E}{\int_{0}^{\infty} \exp(-E/kT)\,\mathrm{d}E} = \exp\left(\frac{-E_0}{kT}\right) \quad (1)$$

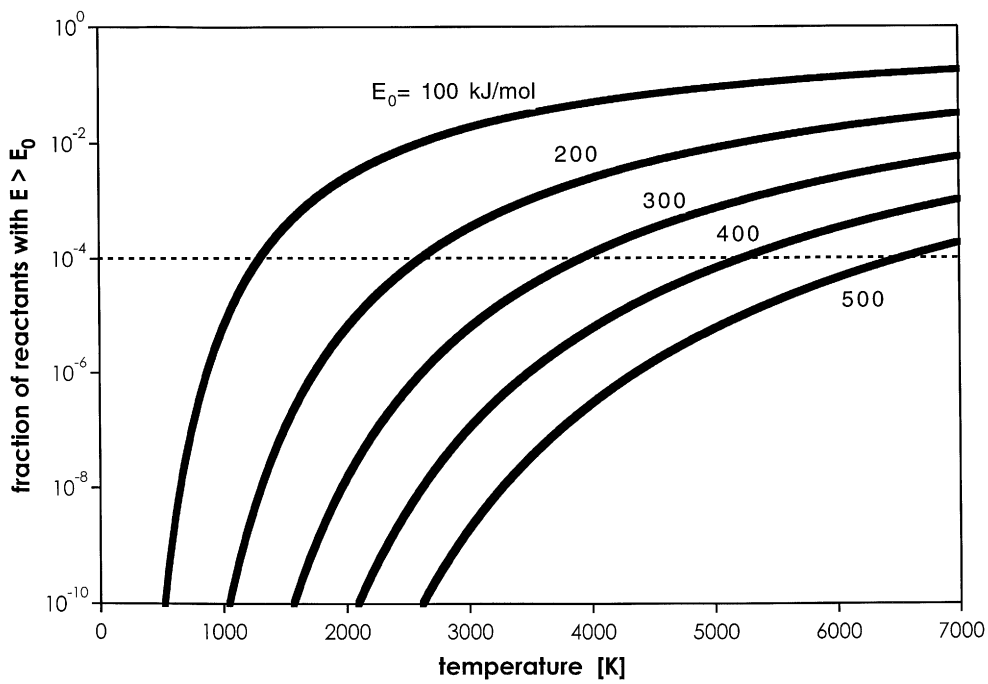

Fig. 5. Relative fraction of reactants from Boltzmann energy distributions that have energies higher than 100, 200, 300, 400, and 500 kJ/mol, respectively, as a function of temperature (calculated from Eq. (1)). The dashed line indicates an ion/neutral ratio of 10^{-4} (or 0.01%), as is typical in UV-MALDI.

where E is the energy, $N(E > E_0)$ the number of molecules with energies $E > E_0$, and N_{total} the total number of molecules, T the temperature, and k is the Boltzmann constant. Reactions which are endoergic by 300 kJ/mol yield an ion/neutral ratio of 10^{-4} at a temperature of 3920 K. This is the ion/neutral ratio which has been experimentally determined for UV-MALDI [36]. Clearly even in the most favorable cases, temperatures far too high to allow the thermally labile analyte molecules stay intact would be required for sufficient ground-state proton transfer in MALDI. Measured plume temperatures are also lower, about 500 K [37]. The temperatures reached in the primary steps are limited by the energy deposition by the laser. Everything from simple estimations to sophisticated molecular dynamics simulations [38,39] shows that this temperature cannot approach the range necessary to make ground-state proton disproportionation reactions significant. This does not rule out primary ionization mechanisms involving proton transfer in general, but shows that they must involve transient non-equilibrium species, such as excited states of some kind.

3.5. Relevance of the data to other recent ionization models

Parallel to the picture presented here and in [7], some authors have proposed a MALDI ionization model involving solvated, preformed ions. In their picture, analytes are initially ionized in solution (e.g., protonated basic protein residues at low pH), incorporated as solvated ions into the crystal with counterions in the vicinity (but only limited direct charge association), and ejected as charged clusters with an excess or deficit of counterions. The final observed ions are thought to be partially neutralized by reaction with oppositely charged species (e.g., electrons to reduce multiply charged cations) or proton transfer reactions, and liberated by subsequent evaporation of the matrix in the plume [40]. However, the results presented here and elsewhere cannot be explained by these models.

First, the preformed ion model cannot predict the matrix suppression effect. In that model analyte and matrix ions are independent, so raising the analyte concentration in a sample can have no effect on the matrix signal.

Second, the preformed ion model places large emphasis on multiply charged ions from solution being statistically neutralized in the plume. This should lead to a charge state distribution that varies depending on the efficiency of the in-plume neutralization step. As the plume becomes less dense, doubly or triply charged ions should be more prevalent. At lower laser fluences (corresponding to lower plume densities), down to the detection threshold of our instrument, no change in the charge state distribution of GGH was observed. If multiply charged analyte is liberated from the MALDI sample as suggested by other authors [5], doubly protonated GGH, carrying protons both at the histidine residue and the N-terminus, $(GGH + 2H)^{2+}$ should become dominant at lowest fluence. However, even at lowest fluence no doubly charged GGH ions were observed.

In contrast, the results are completely consistent with the thermodynamic considerations presented in [7]. Doubly or higher charged ions are not stable with respect to reaction with neutral matrix, unless the individual charge sites are physically quite separated. Small multiply charged species will therefore not even survive in the solid matrix prior to desorption!

It should also be noted that reference [5] proposes electrons to be the dominant reductant. This is considered unlikely since most electrons in MALDI have recently been shown to be photoemission products from contaminated metal surfaces [41]. In the experiments reported here electron emission from the relatively thick sample preparations was not observed, as confirmed in reference experiments on a time-of-flight instrument.

Third, the charge neutralization model is incapable of explaining the negative ion spectra. In particular, the unusual simultaneous matrix suppression in both polarities with SA matrix at higher fluences apparently lies completely outside the charge neutralization model, but is readily and comprehensively predicted by thermodynamics.

Finally it should be made clear that the present model (and that of [7]) does not exclude the possibility

that preformed ions contribute to the MALDI mass spectrum. In certain cases, such as cationization by metal ions, this may be very common. However, the present model proposes that these ions, as well as any created by other primary events, are always subject to further reaction in the plume. These secondary reactions may determine the mass spectrum which will be observed.

4. Conclusions

Matrix–analyte systems exhibiting different proton transfer energetics were examined to probe the role of thermodynamics in determining the final ion distributions in MALDI mass spectra. Relative yields of matrix species and analyte ions strongly depend on the laser fluence used in the MALDI experiment, and ion distributions at fluences not too near threshold are consistent with ground state proton transfer thermochemistry, even for the complex system of ions observed with sinapic acid matrix. Under these conditions in-plume collisions apparently allow ion–molecule thermodynamical equilibrium to be approached, whereas at near-threshold fluences the ion distributions appear to be kinetically limited.

The data shown here are strong evidence that secondary reactions can determine final ion distributions in MALDI. Conversely, ground state disproportionation primary mechanisms do not significantly contribute to the observed ion distributions, as expected from the thermal nature of such processes, and the relatively low temperatures believed to prevail in UV-MALDI experiments. This does not rule out non-thermal proton transfer primary mechanisms.

Acknowledgements

The authors thank the Kommission für Technologie und Innovation (KTI, grant no. 3165.1) and the Austrian Science Fund (FWF, project P15767) for financial support.

References

[1] M. Karas, D. Bachmann, U. Bahr, F. Hillenkamp, Int. J. Mass Spectrom. 78 (1987) 53.
[2] M. Karas, F. Hillenkamp, Anal. Chem. 60 (1988) 2299.
[3] M. Karas, U. Bahr, A. Ingendoh, F. Hillenkamp, Angew. Chem. Int. Ed. Engl. 6 (1989) 760.
[4] M. Glückmann, M. Karas, J. Mass Spectrom. 34 (1999) 46.
[5] M. Karas, M. Glückmann, J. Schäfer, J. Mass Spectrom. 35 (2000) 1.
[6] G.R. Kinsel, M.E. Gimon-Kinsel, K.J. Gillig, D.H. Russell, J. Mass Spectrom. 34 (1999) 684.
[7] R. Knochenmuss, A. Stortelder, K. Breuker, R. Zenobi, J. Mass Spectrom. 35 (2000) 1237.
[8] V.L. Talrose, M.D. Person, R.M. Whittal, F.C. Walls, A.L. Burlingame, M.A. Bldwin, Rapid Commun. Mass Spectrom. 13 (1999) 2191.
[9] S. Alimpiev, S. Nikiforov, V. Karavanskii, T. Minton, J. Sunner, J. Chem. Phys. 115 (2001) 1891.
[10] R. Zenobi, R. Knochenmuss, Mass Spectrom. Rev. 17 (1998) 337.
[11] K. Breuker, R. Knochenmuss, R. Zenobi, J. Am. Soc. Mass Spectrom. 10 (1999) 1111.
[12] K. Breuker, R. Knochenmuss, R. Zenobi, Int. J. Mass Spectrom. 184 (1999) 25.
[13] T.J.D. Jørgensen, G. Bojesen, H. Rahbek-Nielsen, Eur. Mass Spectrom. 4 (1998) 39.
[14] R.D. Burton, C.H. Watson, J.R. Eyler, G.L. Lang, D.H. Powell, M.Y. Avery, Rapid Commun. Mass Spectrom. 11 (1997) 443.
[15] R.J.J.M. Steenvoorden, K. Breuker, R. Zenobi, Eur. Mass Spectrom. 3 (1997) 339.
[16] G.S. Amstrong, M. Peschke, J.S. Klassen, in: Proceedings of the Poster Presentation at the 46th ASMS Conference on Mass Spectrometry and Allied Topics, Orlando, FL, 1998.
[17] S.R. Carr, C.J. Cassady, J. Am. Soc. Mass Spectrom. 7 (1996) 1203.
[18] G.S. Gorman, J.P. Speir, C.A. Turner, I.J. Amster, J. Am. Chem. Soc. 114 (1992) 3986.
[19] G.S. Gorman, I.J. Amster, Org. Mass Spectrom. 28 (1993) 437.
[20] A.G. Harrison, Mass Spectrom. Rev. 16 (1997) 201.
[21] J.W. McKiernan, C.E.A. Beltrame, C.J. Cassady, J. Am. Soc. Mass Spectrom. 5 (1994) 718.
[22] R.A.J. O'Hair, J.H. Bowie, S. Gronert, Int. J. Mass Spectrom. 117 (1992) 23.
[23] Z. Wu, C. Fenselau, Tetrahedron 49 (1993) 9197.
[24] K. Zhang, D.M. Zimmerman, A. Chung-Phillips, C.J. Cassady, J. Am. Chem. Soc. 115 (1993) 10812.
[25] E.M. Marzluff, S. Campbell, M.T. Rodgers, J.L. Beauchamp, J. Am. Chem. Soc. 116 (1994) 7787.
[26] T.W.D. Chan, A.W. Colburn, P.J. Derrick, Org. Mass Spectrom. 26 (1991) 342.
[27] R. Knochenmuss, F. Dubois, M.J. Dale, R. Zenobi, Rapid Commun. Mass Spectrom. 10 (1996) 871.

[28] R. Knochenmuss, V. Karbach, U. Wiesli, K. Breuker, R. Zenobi, Rapid Commun. Mass Spectrom. 12 (1998) 529.
[29] K. Dreisewerd, M. Schürenberg, M. Karas, F. Hillenkamp, Int. J. Mass Spectrom. 141 (1995) 127.
[30] S.G. Lias, J.E. Bartmess, in: W.G. Mallard, P.J. Linstrom (Eds.), NIST Chemistry WebBook, NIST Standard Reference Database Number 69, November 1998, National Institute of Standards and Technology, Gaithersburg MD, 20899 (http://webbook.nist.gov, 1998).
[31] S.G. Lias, J.E. Bartmess, J.F. Liebmann, J.L. Holmes, R.D. Levin, W.G. Mallard, J. Phys. Chem. Ref. Data 17 (Suppl. 1) (1988) 1.
[32] J.E. Bartmess, in: W.G. Mallard, P.J. Linstrom (Eds.), Negative Ion Energetics Data, National Institute of Standards and Technology (http://webbook.nist.gov), Gaithersburg, MD, 1997.
[33] C.M. Nelson, L. Zhu, W. Tang, L.M. Smith, K. Crellin, J. Berry, J.L. Beauchamp, SPIE 2680 (1996) 247.
[34] V. Karbach, R. Knochenmuss, Rapid Commun. Mass Spectrom. 12 (1998) 968.
[35] Q. Lin, R. Knochenmuss, Rapid Commun. Mass Spectrom. 15 (2001) 1422.
[36] C.D. Mowry, M.V. Johnston, Rapid Commun. Mass Spectrom. 7 (1993) 569.
[37] C.D. Mowry, M.V. Johnston, J. Phys. Chem. 98 (1994) 1904.
[38] A. Benscura, V. Navale, M. Sadeghi, A. Vertes, Rapid Commun. Mass Spectrom. 11 (1997) 679.
[39] L.V. Zhigilei, Appl. Phys. A (2002), in press.
[40] R. Krüger, A. Pfenninger, I. Fournier, M. Glückmann, M. Karas, Anal. Chem. 73 (2001) 5812.
[41] M.V. Gorshkov, V.E. Frankevich, R. Zenobi, Eur. J. Mass Spectrom. 8 (2002) 67.